parameter characterizing the 'strength' of the impurity potential controls the RG-flow. The unified plot of the flow diagram is rather rich. The flow diagram contains a new attractive fixed line, L_f, controlling the low temperature physics when the bare potential of the impurity is weak. The existence of the attractive line L_f at an intermediate value of the parameter u_-, follows from the fact that both limiting lines L_∞ and L_0, have proved to be unstable. The presentation of the phase diagram in the space of parameters characterizing the impurity potential, helps clarify the difference between the D_0- and the L_f- lines of fixed points — they are located in different parts of the phase diagram.

The scenario of Ref. [4] is based on the assumption of scaling from a weak impurity scattering to a strong barrier. The existence of the novel line of fixed points, the L_f-line, indicates that the situation is more complicated (see Figs 2a, 2b). We believe that the physics of the L_f-line (that is different from the physics of two weakly connected semi-infinite lines described by D_0) may be related to the strengthening of the role of the Friedel oscillations in the TL model [5]. We think that the attraction to L_f, but not to D_0, is the reason for the results obtained by means of the Coulomb gas theory for the tunneling density of states and the Fermi edge singularity [7, 8].

To conclude, we identify a new attractive fixed point controlling the strong coupling regime of the backward scattering by a single local defect in the TL model. This novel point may also have implications for some other related problems, in particular to the theory of the motion of a quantum particle in a dissipative environment. For a more detailed version of the paper see Ref. [17].

Acknowledgments. We thank D E Khmel'nitskiĭ and Y Gefen for useful discussions. A F is supported by the Barecha Fund Award. This work is supported by the Israeli Academy of Sciences under the Grant No. 801/94-1 and by German–Israeli Foundation (GIF).

References

1. Mattis D C (Ed.) *The Many — Body Problem: an Encyclopedia of Exactly Solved Models in one Dimension* (Singapore: World Scientific, 1993) Ch. 4
2. Wen X-G *Phys. Rev. B* **44** 5708 (1991)
3. Mattis D C *Phys. Rev. Lett.* **32** 714 (1974)
4. Kane C L, Fisher M P A *Phys. Rev. Lett.* **68** 1220 (1992); *Phys. Rev. B* **46** 15233 (1992)
5. Matveev K A, Yue D, Glazman L I *Phys. Rev. Lett.* **71** 3351 (1993)
6. Furusaki A, Nagaosa N *Phys. Rev. B* **47** 4631 (1993)
7. Oreg Y, Finkel'stein A M *Phys. Rev. Lett.* **76** 4230 (1996)
8. Oreg Y, Finkel'stein A M *Phys. Rev. B* **53** 10928 (1996)
9. Eggert S, Affleck I *Phys. Rev. B* **46** 10866 (1992)
10. Affleck I, Ludwig A W *J. Phys. A: Math. Gen.* **27** 5375 (1994)
11. Guinea F *Phys. Rev. B* **32** 7518 (1985)
12. Fradkin E, in *Field Theories of Condensed Matter Systems* (Frontiers in Physics Vol. 82) (Redwood City, Calif: Addison-Wesley Pub. Co., 1991) Ch. 4
13. Nozieres Ph, Blandin A *J. Phys.* (Paris) **41** 193 (1980)
14. Matveev K A *Phys. Rev. B* **51** 1743 (1995)
15. Emery V J, Kivelson S *Phys. Rev. B* **46** 10812 (1992)
16. Affleck I et al. *Phys. Rev. B* **45** 7918 (1992)
17. To be published in *Philosophical Magazine, in the Proceedings of the "Minerva Workshop on Mesoscopics, Fractals and Neural Networks", Eilat, Israel, March 1997* (cond-mat/9707162)

Ground states in one-dimensional electron systems

W Hansen, D Schmerek, C Steinebach

The screening properties of a low-dimensional electron system in heterostructures can be rather directly probed by measurement of the capacitance between a metallic front electrode and the electron system. In this way very valuable information on the density of states (DOS) of the electron system are acquired as demonstrated in a number of publications on the DOS in electron systems of two [1, 2] or even fewer [3–7] dimensions. For an unambiguous and even quantitative analysis of the data it is crucial that the time in which charge equilibrium in the system is established is much shorter than the period over which the capacitance signal is measured. This is generally not the case if the charge exchange takes place by transport within the low-dimensional system. At high magnetic fields the capacitance signal then incorporates transport properties in the electron system with peculiar behavior at even filling factors where the diagonal conductivity vanishes [8–11]. On the other hand special heterojunction devices are developed that contain a back contact from which charge injection into the low-dimensional electron system takes place at high rates even in high magnetic fields. In this contribution we would like to summarize a number of experiments performed on such devices with electron channels of different widths. The results demonstrate that the gate voltage dependence of the capacitance reflects the formation of edge states [12, 13] and — at even smaller channel width — spatial quantization into one-dimensional (1D) subbands.

In Figure 1 a cross section and a top view of the metal insulator semiconductor (MIS) devices used for our experiments is sketched. The heterojunction samples are grown by molecular beam expitaxy and contain an Si-doped back contact, a GaAs spacer, a barrier formed by an AlAs/GaAs superlattice a thin GaAs cap layer and thermally evaporated gate electrodes that are finely patterned by electron beam lithography [6]. The layer thicknesses of the GaAs spacer layer, the barrier and the cap are 100 nm, 37 nm and 5 nm, respectively. The gate electrodes form a 150 μm long center

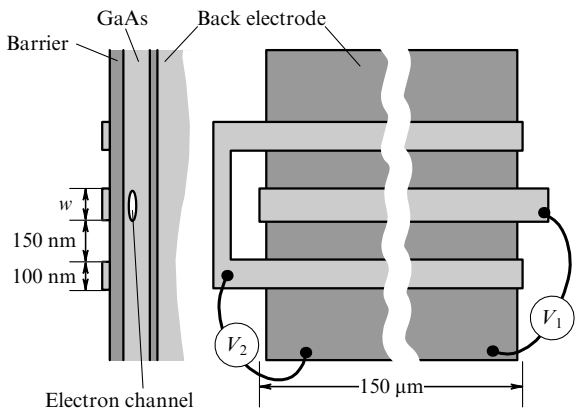

Figure 1. Cross section and top view of a MIS heterojunction device for the investigation of narrow electron channels. In the top view light areas represent the front electrodes and the dark area — the back contact. The thicknesses of the barrier and the separation between the gate and back electrode are, respectively: $d = 42$ nm and $D = 142$ nm.

electrode of width w that is enclosed by a tuning fork shaped electrode. The latter essentially consists of two side gates running parallel to the center electrode at a distance of 150 nm. In our devices the barrier is undoped to minimize potential fluctuations in the electron channel under investigation. The gates are biased at different voltages V_1 and V_2 with respect to the back electrode. The electron channel is created beneath the center gate at gate voltages V_1 larger than a threshold voltage $V_{\rm th}$. Whereas the center electrode mainly controls the electron density in the channel the confinement potential is tuned by the voltage V_2 applied to the side gates [14].

Typical capacitance gate voltage traces of devices with different widths of center electrode are presented in Fig. 2. The sudden rise of the capacitance denotes the threshold voltage at which the electron channel is created. Threshold voltages are found to increase with decreasing gate width. In Figure 2 the gate voltage scales of the different devices are offset in order to make comparison convenient. For the same reason the capacitances of the devices are normalized to similar values. A magnetic field $B = 6$ T is applied perpendicular to the sample surface. The dashed line depicts the capacitance of a device with a wide gate so that the channel edge does not contribute to the signal. A pronounced minimum at $V_1 - V_{\rm th} = 0.23$ V denotes the gate voltage at filling factor $\nu = 2$ where the chemical potential traverses the Landau gap in the DOS. A much less pronounced minimum at $V_1 - V_{\rm th} = 0.11$ V is associated with filling factor $\nu = 1$ where the chemical potential traverses the much smaller spin gap. The DOS in the Landau and spin gap have been thoroughly investigated in a similar device in recent publications [2, 15, 16]. The full line denotes the capacitance signal recorded on a device with a center gate of width $w = 300$ nm. The potential difference between the side gates and the center gate is kept constant at $\Delta V = V_1 - V_2 = 3.5$ V. It is obvious that the onset of the capacitance at the threshold is much smoother, the capacitance minimum at filling factor $\nu = 2$ is asymmetric and shifted to higher gate voltages. These features can be understood in a simple model that considers the contribution of the edge states to the capacitance signal [14, 17]. The dashed line presents the capacitance of a device with gate width $w = 100$ nm and will be discussed in more detail later.

Whereas in a bulk two-dimensional (2D) device the form of the capacitance minimum is always symmetric and determined by the defect-induced DOS in the whole device [15], in the small $w = 300$ nm device we expect the edge states to significantly contribute to the capacitance minimum. It is well known that the screening properties of the electrons in the edge states lead to the formation of compressible electron stripes at the edge of the 2D device [12, 18]. They are separated by a number of incompressible stripes that is equal to the number of Landau gaps below the Fermi energy. In our simple, semi-quantitative model the compressible stripes contribute to the measured capacitance like perfect metallic electrodes whereas the incompressible stripes do not. We assume that the capacitance is proportional to the area of the compressible stripes, which is a good approximation as long as the distance between the electron system and the gate is smaller than the width of the compressible stripes.

The capacitance thus approximately reflects the geometry of the compressible stripes as indicated by the inserts in Fig. 3. Here the capacitance is depicted together with the result of our model for gate voltages at which the system is close to filling factor $\nu = 2$. If spin splitting is neglected, the channel form a single compressible stripes at filling factors $\nu < 2$ with a width determined by the confinement potential [17]. In particular, a smooth confinement potential results in a smooth increase of the capacitance, which explains the strikingly smoother onset of the capacitance of the $w = 300$ nm device although the gate area of the sample is just 6% of the bulk 2D sample. In our model we expect the capacitance to be maximal at a gate voltage at which in the center of the channel the local density is at filling factor $\nu = 2$. In contrast the bulk device exhibits a minimum precisely at $\nu = 2$ reflecting the low DOS in the cyclotron gap. This nicely demonstrates that in our $w = 300$ nm device edge states predominantly determine the capacitance signal rather than

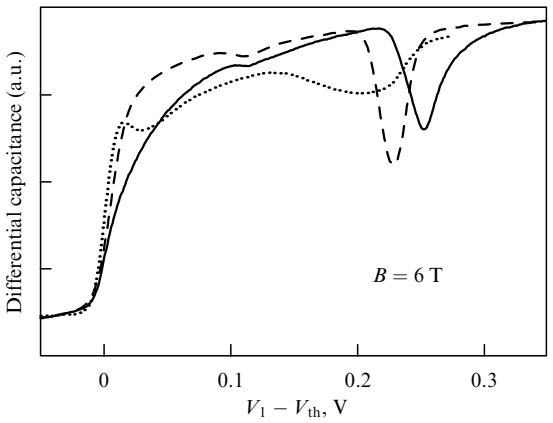

Figure 2. Differential capacitance measured as a function of the gate voltage in devices of different gate width at $B = 6$ T. The capacitance signals are normalized to similar values at $V_1 - V_{\rm th} = 0.35$ V in order to make comparison possible. The dashed line presents the differential capacitance of a 2D sample with wide gates, so that the edge channels do not significantly contribute to the signal. The full line is recorded in a device with $w = 300$ nm at $\Delta V = 3.5$ V and the dotted line with $w = 100$ nm at $\Delta V = 1.0$V, respectively.

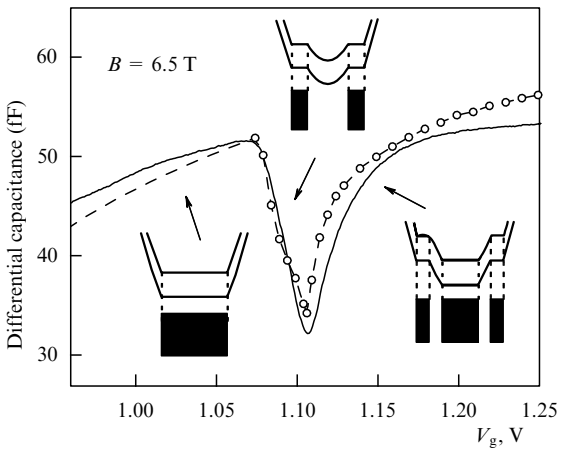

Figure 3. Differential capacitance of the $w = 300$ nm device close to the gate voltages at which the second Landau level starts to become occupied. The inserts sketch the screened confinement potential and the geometry of the compressible stripes at gate filling factors below, about equal to and above 2. The bias between the center gate and side gates $\Delta V = 3.2$ V. The dashed line and open circles are calculated in a model described in the text.

the defect induced DOS as is the case in wider channels. At higher voltages an incompressible gap arises in the channel center as indicated by the top insert and leads to a steep decrease of the capacitance. The capacitance drops until a further compressible stripe arises in the center of the channel that is associated with the second Landau level. The width of the central stripe changes much faster than the area of the incompressible stripes giving rise to a smooth increase of the capacitance signal similar to that at the onset.

The dashed line and open dots denote the results of our model calculations. The external confinement potential used for the calculation was determined numerically with a Poisson solver with boundary conditions dictated by the potentials of the gates. The exposed surfaces between the gates are treated as a dielectric interface with no additional surface charges [14]. The agreement between measurement and model is quite good.

From the dotted line in Fig. 2 it is obvious that the gate voltage dependence of the capacitance changes completely if the channel width is reduced even further, so that size quantization becomes important. The onset is even steeper than that of the two-dimensional sample. It has a small dent at a slightly higher gate voltage and a larger one close to gate voltages where in wider channels the density corresponds to a filling factor $\nu = 2$. A structure associated with spin splitting is not observed in this trace but becomes visible in greater magnetic fields or at lower temperatures [19].

In Figure 4 the capacitance of the $w = 100$ nm device is recorded at different magnetic fields. In contrast to the behavior of 2D devices the capacitance trace exhibits an already pronounced structure at zero magnetic field. Both the dent close to the onset and steps in the capacitance can be clearly resolved. It has been shown [6, 19] that the steps reflect the onsets of the 1D subbands in the channel as indicated in Fig. 4. From magneto-capacitance measurements, for gate voltages below the onset of the second subband we determine typical average subband spacings of 4–5 meV with a parabolic confinement model. From far infrared absorption experiments we determine 6–10 meV for the level spacing in the unscreened confinement potential.

From comparison of the traces in Fig. 4 it is obvious that the capacitance minimum observed in Fig. 2 is associated with the onset of the second 1D hybrid subband. Even at high magnetic fields where the magnetic length becomes smaller than the channel width the asymmetry of the capacitance minimum obviously remains very distinct from that in wider channels.

From Figure 4 it is also clear that the structure at the onset of the quantum wire also exists at zero magnetic field. In our two-dimensional devices such a structure is not observed. At present the origin of this structure is not fully clear. However, numerical simulation calculations indicate that it may be the result of interaction effects. Typical results of such calculations are presented in Fig. 5 for gate voltages very close to the threshold voltage. The potential and electron density distributions in the quantum wire are calculated with a self-consistent Schrödinger–Poisson solver. Electron–electron interaction effects are included in a local density approximation [20]. Boundary conditions are determined by the applied gate voltages. At the exposed crystal surface between the center and side gate electrodes we assume the Fermi energy to be pinned at the midgap position [21].

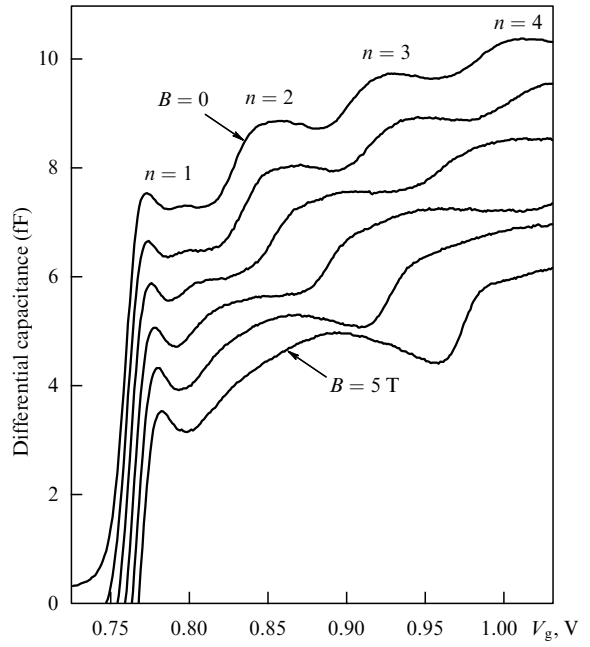

Figure 4. Differential capacitance of a $w = 100$ nm device recorded at magnetic fields applied perpendicular to the wires. The topmost trace is recorded at $B = 0$ T. The lower traces are offset for clarity and recorded at fields increasing in steps of 1 T. Indices denote the one-dimensional subbands that start to become occupied in the steps of the $B = 0$ T trace.

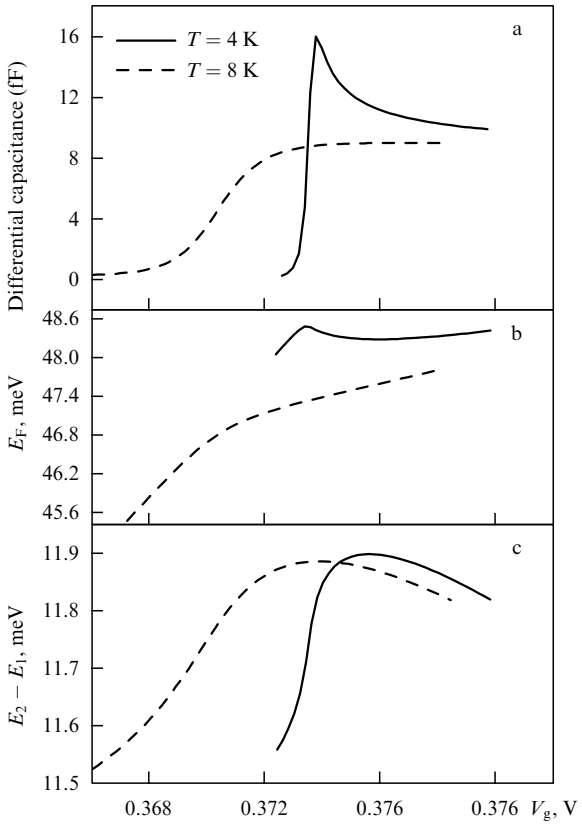

Figure 5. (a) Differential capacitance, (b) Fermi energy and (c) subband separation calculated with a self-consistent Schödinger–Poisson solver for a $w = 100$ nm sample at gate voltages very close to the threshold of the quantum wire. It is assumed that no magnetic field is applied, $\Delta V = 2.0$ V and that there is just thermal but no inhomogeneous broadening.

In Figure 5a the thus calculated differential capacitance is depicted for temperatures $T = 4$ and 8 K. At the lower temperature the capacitance rises steeply and is clearly enhanced in the onset region. At higher temperature the enhancement is washed out. The origin of the enhancement can be identified with the help of Fig. 5b and 5c, where the Fermi energy and the energy separation between the first and second 1D subband are depicted, respectively. If the quantum wire just starts to become filled with electrons the Fermi energy drops at low temperature and the energy separation between the subbands increases. Neither feature is expected in a Hartree calculation [22]. However, a qualitatively similar behavior is predicted in analytical calculations that include exchange-correlation effects [23]. In addition, it is well known from experiments on 2D systems that many-particle effects can lead to so-called 'negative compressibility' giving rise to an enhanced capacitance [24, 25]. Such effects are observable in our 2D devices at high magnetic field and low temperatures [26]. The fact that they are less pronounced indicates that correlation effects are much more important in 1D electron systems.

In summary, we present capacitance measurements on electron channels of different widths in the range where we expect a transition from 2D to 1D behavior. In wide channels the typical 2D behavior is found. Pronounced and symmetric capacitance minima at even filling factors reflect the reduced DOS in the cyclotron gap that is dependent on impurity induced potential fluctuations in the bulk of the device. In contrast the capacitance of 300 nm wide channels is dominated by the influence of the confinement on the width of the compressible electron stripes at the channel edge. The onset of the capacitance is considerably smoother than in wide channels and the minimum at integer filling factors is asymmetric. At even smaller channel width the capacitance reflects the spatial quantization into one-dimensional subbands. The shape of the capacitance minima is strikingly different to that of wider channels, the onset becomes steep again and it exhibits additional structure. Simulation calculations indicate that the observed enhanced capacitance at the onset reflects the importance of the exchange energy in the ground state of quantum wires in the one-dimensional quantum limit.

Acknowledgments. We benefited from invaluable technical support from S Manus and many discussions with A O Govorov, J P Kotthaus, and V T Dolgopolov. We gratefully acknowledge financial support of the Deutsche Forschungsgemeinschaft through project Ha2042/2-2 and the Graduiertenkolleg "Physik nanostrukturierter Festkörper".

References

1. Smith T P et al. *Phys. Rev. B* **32** 2696 (1985); Smith T P III, Wang W I, Stiles P J *Phys. Rev. B* **34** 2995 (1986).
2. Dorozhkin S I et al. *Usp. Fiz. Nauk* **168** 135 (1998) [*Sov. Phys. Usp.* **41** 127 (1998)]; Dolgopolov V T et al. *Usp. Fiz. Nauk* **168** 147 (1998) [*Sov. Phys. Usp.* **41** 138 (1998)]
3. Smith T P III et al. *Phys. Rev. Lett.* **59** 2802 (1987)
4. Hansen W et al. *Phys. Rev. Lett.* **62** 2168 (1989)
5. Ashoori R C et al. *Phys. Rev. Lett.* **71** 613 (1993)
6. Drexler H et al. *Phys. Rev. B* **49** 14074 (1994)
7. Drexler H et al. *Phys. Rev. Lett.* **73** 2252 (1994)
8. Takaoka S et al. *Phys. Rev. Lett.* **72** 3080 (1994)
9. Chen W et al. *Phys. Rev. Lett.* **73** 146 (1994)
10. Zhitenev N B et al. *Phys. Rev. Lett.* **77** 1833 (1996)
11. Ashoori R C, contribution to this workshop
12. Halperin B I *Phys. Rev.* **B 25** 2185 (1982)
13. Büttiker M, in *Semiconductors and Semimetals* (Eds R K Willardson, A C Beer, E R Weber) Vol. **35** (Ed. M Reed) (San Diego: Academic Press, 1992) p. 191
14. Schmerek D et al. *Phys. Rev. B* **54** 13816 (1996)
15. Dolgopolov V T et al. *Phys. Low-Dim. Struct.* (6) 1 (1996)
16. Dolgopolov V T et al. *Phys. Rev. Lett.* **79** 729 (1997)
17. Govorov A O *Phys. Rev. B* **51** 14498 (1995)
18. Chklovskii D B, Shklovskii B I, Glazman L I *Phys. Rev. B* **46** 4026 (1992); Chklovskii D B, Matveev K A, Shklovskii B I *Phys. Rev. B* **47** 12605 (1993)
19. Hansen W, Drexler H, in *Festkörper probleme* (Advances in Solid State Physics Vol. 35, Ed. R Helbig) (Braunschweig/Wiesbaden: Vieweg, 1996) p. 81
20. Gunnarsson O, Lundqvist B I *Phys. Rev. B* **13** 4274 (1976)
21. Grant R W et al. *J. Vacuum Sci. Technol.* **19** 477 (1981)
22. Laux S E, Frank D J, Stern F *Surf. Sci.* **196** 101 (1988)
23. Gold A, Ghazali A *Phys. Rev. B* **41** 8318 (1990)
24. Eisenstein J P, Pfeiffer L N, West K W *Phys. Rev. Lett.* **68** 674 (1992)
25. Kravchenko S V et al. *Phys. Rev. B* **47** 12961 (1993)
26. Dolgopolov V T et al. *Phys. Rev. B* **51** 7958 (1995)

Pumping of energy into a mesoscopic ring. Exactly solvable model

L Gorelik, S Kulinich, Yu Galperin,
R I Shekhter, M Jonson

1. Introduction

The physical properties of mesoscopic systems are strongly influenced by the quantum interference of electronic states (see, e.g., Ref. [1] and references therein). Anderson localization of electrons, universal fluctuations of conductance as well as the periodic magnetic field dependence of thermodynamical and transport properties of multiply connected devices (e.g., metallic rings) are important examples. Previous extensive studies in mesoscopic physics were concentrated mainly on thermodynamics, as well as on the linear response of nanosrtuctures to dc or electrical and magnetic perturbations slowly varying in time. At the same time, relatively little is known about the *nonlinear* response of mesoscopic systems to a time-dependent bias. In general, an electron driven by an external time-dependent force does not conserve energy. In spite of the non-conservation of energy, interference processes remain crucially important if the phase breaking rate is much less than the rate characterizing *dynamical* redistribution of the electron wave function between different states in the energy space.

Below we consider an example of such a system, namely a single-channel mesoscopic ring subjected to a non-stationary perpendicular magnetic field, linearly dependent on time. We concentrate on the energy accumulation in such a system as a function of time. To investigate the role of interference, we take into account electron backscattering from a single potential barrier ('defect'), embedded in the ring. It is shown that by tuning either the time derivative of the external magnetic field variation, or the transmission amplitude through the barrier (by the gate potentials), one can influence the interference pattern, and in this way significantly change the dynamics. Impure conducting rings have been extensively discussed in connection with energy dissipation in mesoscopic *metallic* systems [2]. Gefen and Thouless [3, 4] have suggested that randomly distributed impurities lead to the so-called